FREDERICK C. JACKSON

THE RADAR OCEAN-WAVE SPECTROMETER

The scanning-beam radar ocean-wave spectrometer (ROWS) technique is described and a "strawman" design for a ROWS mode on Spectrasat is presented. In the proposed design, two pencil beams separated by a few degrees in elevation are used to measure the cross-section roll-off. In addition to providing the requisite data for the tilt sensitivity, these measurements will provide a means of estimating the wind vector over the swath.

INTRODUCTION

The scanning-beam radar ocean-wave spectrometer (ROWS) technique had its origins in the early 1970s when NASA was considering various possibilities for a waves sensor on Seasat. At that time the Goddard Space Flight Center (GSFC) proposed a conceptually simple but totally unproven approach as an alternative to synthetic aperture radar (SAR). In essence, this approach was to use an off-nadir-pointing, conically scanning, short-pulse radar to measure the wave-associated surface contrast variations as a function of surface range and antenna azimuth. Spectrum analysis of the returned signal as a function of range on the surface would yield a measure of the wave-slope spectrum for that azimuth; wave direction would be determined by the azimuth at which the signal spectrum was greatest. At that azimuth, the wave crests would be aligned with the electromagnetic wave front striking the surface, and so the contrast signal would be maximized. It was suggested that short-pulse altimeters such as the one planned for Seasat could be modified to perform the measurement. The altimeter would have adequate link margin provided the nadir angle was not too large, and angles around 10 degrees were considered. Small-angle operation was also seen to be desirable in order to keep the scan radius reasonably small. While the concept was promising, there was no real theory of measurement and no supporting aircraft data at the time, and so NASA understandably chose to fly a SAR on Seasat.

GSFC, however, continued its interest in the short-pulse scanning-beam concept. In 1974 an aircraft instrument development program was begun based on breadboard Geos-C altimeter hardware, and subsequently considerable effort was also devoted to developing a rational theory of measurement.[1] Aircraft data obtained with the GSFC Ku-band chirped radar in 1978 provided the proof of concept. Analysis of these data, obtained with a small rotating antenna at altitudes between 5 and 10 kilometers, showed that absolute, directional wave-height spectra could be measured with remarkable accuracy.[2,3] The aircraft data were shown to scale in accordance with the theory, and thus the feasibility of a ROWS measurement at spacecraft altitudes was fairly well assured. Since 1978, the Goddard ROWS instrument has flown on several missions on the NASA P-3 with the surface contour radar (see Walsh et al., this issue). Among the more recent missions is the SIR-B underflight mission discussed by both Beal and Monaldo elsewhere in this issue.

In the following, we describe briefly the ROWS measurement technique and present some examples of the aircraft data; then we present a preliminary "strawman" design for a ROWS mode on Spectrasat.

Frederick C. Jackson is a research scientist in the Laboratory for Oceans, NASA/Goddard Space Flight Center, Greenbelt, MD 20771.

ROWS TECHNIQUE

The ROWS geometry is shown in Fig. 1. Short pulses (or equivalent pulse-compression waveforms) are transmitted, strike the sea surface, and backscatter some of the energy to the receiver. The pulses are assumed to be short enough to resolve the dominant waves. The backscattered pulses are detected, integrated (in range bins fixed in the surface), and then subjected to spectrum analysis for the spectrum of the reflectivity modulation as a function of range. Because of the large lateral extent of the antenna footprint (e.g., L_y = 8 kilometers for Spectrasat), the wave contrasts cannot be resolved in azimuth (short of resorting to synthetic aperture). Rather, the wave contrasts are averaged laterally across the beam spot. This averaging provides the directional resolution, since only surface-contrast wave components aligned with the beam direction will contribute to a net contrast signal. The condition is essentially one of wave-front matching, the same that provides the directional resolution in the two-frequency scanning-beam technique (cf. Refs. 1 and 4; also Plant, this issue). The mechanism of contrast modulation by the dominant waves depends on the incidence angle, θ. At large angles, $\theta \gtrsim 20$ degrees, the predominant mechanisms of contrast variation are hydrodynamic and aerodynamic

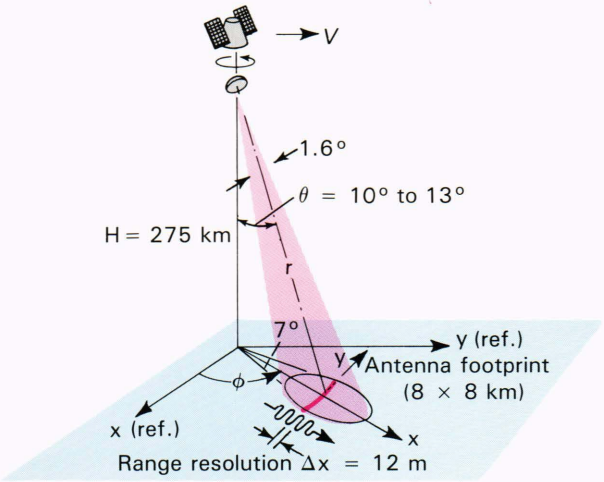

Figure 1—Schematic of the ROWS concept, using a narrow pulse radar to irradiate the surface from a circularly scanning off-nadir antenna.

modulation of the short Bragg-diffracting wavelets; geometrical tilting is generally less important. The opposite is the case in near-nadir backscatter, $\theta \lesssim 15$ degrees; here geometrical tilting provides most of the signal. The scattering is quasi-specular, and the contrast mechanism is similar to that in sun glint observations. (No doubt the reader has observed waves in the sun's glint pattern from an airplane and noticed the high visibility of waves running orthogonal to the isophotes.)

A geometrical optics solution for the spectrum of the range reflectivity modulation is given in Ref. 1; an alternative derivation of the solution is given in the companion paper by the author in this issue. In both papers and in Ref. 2, the conditions under which the scattering solution may be linearized to yield proportionality to the slope spectrum are described; in Ref. 1 the results of some second-order calculations for scattering from a Gaussian sea surface are given. The calculations indicate that, overall, the combined effect of harmonic distortions arising from the steep aspect angle and from the "bursty" character of infrequent steep specular slopes tend to be a minimum for an angle of incidence near the root-mean-square slope (about 10 degrees for a 10-meter-per-second wind); also, the more gentle the dominant wave slopes and the higher the root-mean-square slope (or wind speed), the greater is the fidelity of the contrast spectrum to the large-wave slope spectrum. If the surface-wave vector is defined as

$$\mathbf{k} = 2(2\pi f/c) \sin\theta \, (\cos\phi, \sin\phi) ,$$

where f is the detected video modulation frequency, c the speed of light, θ the incidence angle, and ϕ the azimuth angle, then the reflectivity modulation spectrum in the linear approximation may be expressed as

$$P_m(\mathbf{k}) = \alpha \, |\mathbf{k}|^2 \, F(\mathbf{k}) \qquad (1a)$$

where $F(\mathbf{k})$ is the polar symmetric height spectrum defined such that the height variance

$$\langle \zeta^2 \rangle = \int_0^\infty \int_0^\pi 2F(\mathbf{k}) k dk d\phi ,$$

and where the "sensitivity coefficient" is given by

$$\alpha = \frac{4\sqrt{\pi \ln 2}}{L_y} \left(\cot\theta - \frac{\partial \ln \sigma^0}{\partial \theta} \right)^2 , \qquad (1b)$$

where L_y is the lateral (azimuthal) 3-decibel footprint dimension (for the formulas presented here, Gaussian beam and pulse shapes are assumed), and $\sigma^0 = \sigma^0(\theta,\phi)$ is the average surface cross section. The cot θ term represents a linearized area tilt term (such as would provide the contrast for a wavy Lambertian surface); the second tilt term—the cross-section roll off—represents the rigid rotation of the subresolution-scale scattered-power pattern in the plane of incidence by the large wave slopes. Since σ^0, near vertical incidence, is proportional to the wave-slope probability density function $p(\nabla\zeta)$ evaluated at the specular condition $\nabla\zeta = \tan\theta \, (\cos\phi, \sin\phi)$, it follows that for an approximately Gaussian sea

$$\frac{\partial \ln \sigma^0}{\partial \theta} \simeq \frac{\partial \ln p}{\partial \tan\theta} = -\tan\theta \left[\frac{\cos^2(\phi - \phi_x)}{\langle \zeta_x^2 \rangle} + \frac{\sin^2(\phi - \phi_x)}{\langle \zeta_y^2 \rangle} \right] , \qquad (2)$$

where here x and y are assumed to be the principal axes and where ϕ_x is nominally the wind direction. At Ku-band frequencies (about 2-centimeter wavelength), $\zeta_y^2/\zeta_x^2 \approx 0.85$ typically, and the mean square slope $\langle (\nabla\zeta)^2 \rangle = \langle \zeta_x^2 \rangle + \langle \zeta_y^2 \rangle$ is given approximately by[5]

$$\langle (\nabla\zeta)^2 \rangle \simeq 0.0022 \, U + 0.016 \qquad (3)$$

for neutral 10-meter winds U greater than 6 to 8 meters per second. The slope variance predicted by Eq. 3 is about 60 percent of the optical slope variance; for lower wind speeds, the Ku-band mean-square slope is approximately equal to the optical slope as determined by Cox and Munk.[5]

By definition, the root-mean-square modulation depth is given by

$$\langle m^2(x, \phi) \rangle^{1/2} = \left[\int_0^\infty 2P_m(k, \phi) dk \right]^{1/2} . \qquad (4)$$

For a k^{-2} slope spectrum, it matters little for design purposes whether the upper limit is taken as the resolution wavenumber or infinity.

We note that the wave-front curvature does not affect the form of Eq. 1 provided that the sea is directionally spread, that is, provided that the directional spread of the sea is greater than the wave-front curvature (e.g., 7 degrees in the case of the satellite design to be discussed). In the case of narrowband swells, the $1/L_y$ dependence of the sensitivity coefficient will have

to be modified, and the result of integrating the swell spike over a larger angular band (e.g., an output band of 15 degrees) will have to be established. Let β_θ and β_ϕ represent the elevation and azimuth 3-decibel beamwidths. The 3-decibel range and azimuth footprint dimensions are then given by $L_x = r_0 \sec\theta\, \beta_\theta$ and $L_y = r_0\, \beta_\phi$ where r_0 is the slant range to the beam-spot center. The directional resolution for a stationary beam, defined as the 3-decibel spectral window width (in azimuth), is given by

$$\Delta\phi_{\text{stat}} = \left[\left(\frac{8\ln 2}{kL_y}\right)^2 + (\beta_\phi \csc\theta/2)^2\right]^{1/2}, \quad (5)$$

where the two terms represent, respectively, the effect of the finite footprint and the wave-front curvature. In the case of a rotating beam, one must also factor in the finite azimuth $\Delta\phi_{\text{rot}}$ swept out during the pulse integration time. The resolution in this case needs to be calculated, but it should not be too different from the stationary case since the effective azimuth footprint L_y (data window) is increasing at the same time the effective angular spread $\beta_\phi \csc\theta$ is increasing. The resolution might be conservatively approximated by

$$\Delta\phi \simeq [(\Delta\phi_{\text{stat}})^2 + (\Delta\phi_{\text{rot}})^2]^{1/2} .$$

For steep incidence angles, wave-front curvature can affect the wavenumber resolution. In the plane-wave aproximation, the surface range x is related to the signal delay time τ according to

$$x - x_0 = c\,(\tau - \tau_0)/(2 \sin\theta_0) , \quad (6)$$

where the subscript refers to nominal values at the center of the beam spot. Similarly, the surface wavenumber is proportional to the video-modulation frequency, f, as

$$k = (4\pi f/c) \sin\theta . \quad (7)$$

The linear time-versus-surface-range and frequency-versus-wavenumber relationships will hold for elevation beamwidths of a few degrees. For larger beamwidths (e.g., such as we have in the case of the aircraft ROWS, $\beta_\theta = 10$ degrees, $\beta_\phi = 4$ degrees), one must correct for wave-front sphericity. In a short pulse system, this can be done by re-arraying the time-domain sampled data (the detected power versus delay time) according to

$$H^2 + x^2 = [H + c\,(\tau - \tau_N)/2]^2 , \quad (8)$$

where $H = c\,\tau_N/2$ is the altitude and τ_N is the delay time (epoch time) corresponding to the return of a pulse from the nadir point. This time can be provided by the radar altimeter (RA) segment of a combined altimeter/spectrometer (RA/ROWS) system (see MacArthur, this issue; also below).

For a finite-duration, finite-bandwidth pulse, one must account for the Rayleigh fading (speckle) and the point target response. If the point-target-response spectrum is denoted $R(k)$, then the observed spectrum of a single backscattered, square-law detected pulse is given by

$$P_{N=1}(k, \phi) = R(k) \left[P_m(k, \phi) + \frac{\Delta x}{2\sqrt{2\pi\ln 2}}\right] ,$$

where Δx is the 3-decibel-range-resolution cell (or equivalent bandwidth surface-range resolution). An integration of N independent pulses prior to spectrum analysis will reduce the fading variance by a factor of N. If the platform is moving rapidly, the pulse returns cannot be integrated in radar-fixed range or delay bins but must be integrated in range bins attached to the surface. Assuming that this is accomplished with proper surface tracking, then one has for the signal-to-noise ratio (SNR) of the measured spectrum,

$$\text{SNR}_N = \frac{2\sqrt{2\pi\ln 2}}{\Delta x} \cdot N\, P_m(\mathbf{k}) . \quad (9)$$

One may also account for thermal noise here; however, if the average signal power to thermal-noise power ratio (signal-to-noise ratio) is 3 decibels or greater, thermal noise can be neglected as far as the spectrum measurement is concerned.

Numerous other considerations enter into the practical measurement problem. Most of them are dealt with in Refs. 2 and 3 and are discussed below.

AIRCRAFT DATA

The extensive aircraft flight data set obtained in 1978 with the GSFC Ku-band pulse-compression radar[2,3] has fairly well demonstrated the basic validity of the ROWS technique. The linear-tilt-model prediction has been verified with data obtained between 5 and 10 kilometers altitude, and the ability to measure absolute wave-height spectra over a range of sea states from 2 to 10 meters has been demonstrated. Good fidelity to the slope spectrum is observed up to frequencies approaching twice the peak frequency.

Figure 2 is a dramatic example of ROWS spectra obtained from the 1978 mission. The data—here converted from slope spectra in the wavenumber domain to height spectra in the frequency domain—show two energetic wave systems produced by an intense cyclone travelling up the Norwegian coast (Fig. 3) These data have been used together with data from a Waverider buoy located near the ROWS file A to test the performance of two numerical wave models developed by V. Cardone of Oceanweather, Inc. The results indicate that the hindcasts performed remarkably well considering the intensity and speed (25 meters per second) of the storm. The basic structure and spatial distribution of the ROWS spectra in Fig. 2 were reproduced in the hindcasts. The discrepancies that existed appeared to result from model phasing and/or wind-field errors and possibly from a too-rapid directional relaxation. Figure 4 is an exam-

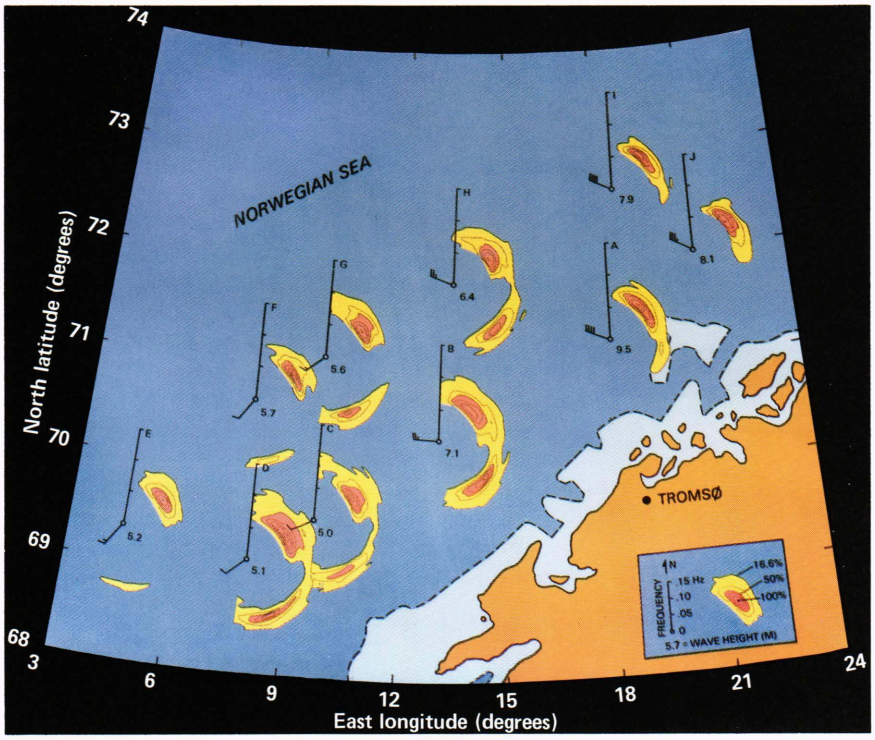

Figure 2—Norwegian Sea storm height-frequency spectra, November 3, 1978, 0800-1000 GMT. The CV-990 aircraft altitude was 10 kilometers. The wind barbs (full barb = 5 meters per second) are from the hindcast wind-field analysis.

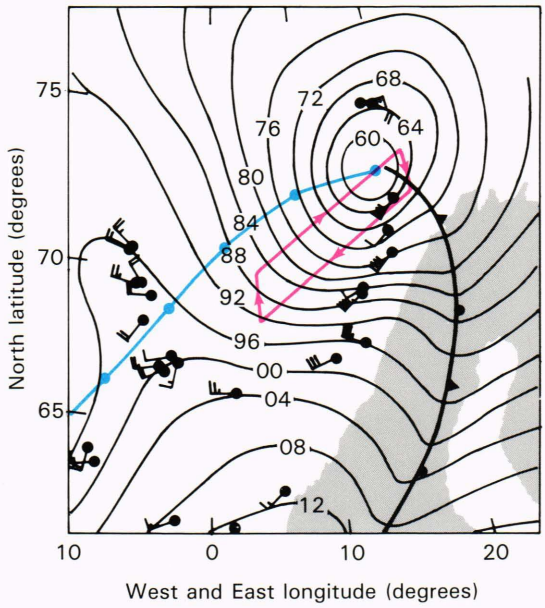

Figure 3—Surface weather chart, 1800 GMT, November 2, 1978, with the CV-990 flight track and low's track, plotted for six-hourly positions.

ple of a three-way comparison among the hindcast, the ROWS spectra, and the buoy spectra. The ROWS and buoy nondirectional spectra are seen to be in excellent agreement. The hindcast closest in time to the observations does not agree well with the observations; however, the hindcast 6 hours earlier does.

Since 1978, the ROWS has flown on several flight experiments on the NASA P-3 in concert with the surface contour radar (SCR) (cf. Walsh et al., this issue) and we have accumulated a sizable intercomparison data set. Probably the most interesting of the data sets obtained so far are of fetch-limited waves off the U.S. east coast. Figure 5 is an example of ROWS data obtained at 6 kilometers altitude over an approximate 200-kilometer fetch normal to the U.S. east coast off Wallops Island, Va. The figure illustrates the profound effect of coastline irregularities on the developing wave field. In this case, Delaware Bay appears to be acting as a source of energetic waves traveling off the wind direction (which was within a few degrees of normal to the coast). Unfortunately, because of a malfunction of the SCR, no comparison data from it are available for this flight; however, SCR radar data obtained in the same location under similar wind conditions two years before[6] compare remarkably well. (Note that the data in Fig. 5 are preliminary; for example, they have been computed assuming an isotropic α.)

Figure 6 is a comparison of ROWS and SCR spectra for a large fetch in a fetch-limited situation on another flight day. Just as it was in the case of Fig. 5, one sees a bimodal wave system with nearly equally energetic downwind and off-wind components despite the fact that the wind was normal to what would seem to be a fairly straight coastline. In this case, the off-wind component is traceable to the apex of the New York Bight (Fig. 6b). The ROWS spectrum, here corrected for a 15-percent anisotropy in the mean-square slope according to Eqs. 2 and 3 with $\langle(\nabla\zeta)^2\rangle = 0.04$, is seen to be in good agreement with SCR. The modal directions, peak values, and half-power contours agree quite well; the approximate 5 percent difference in the downwind component

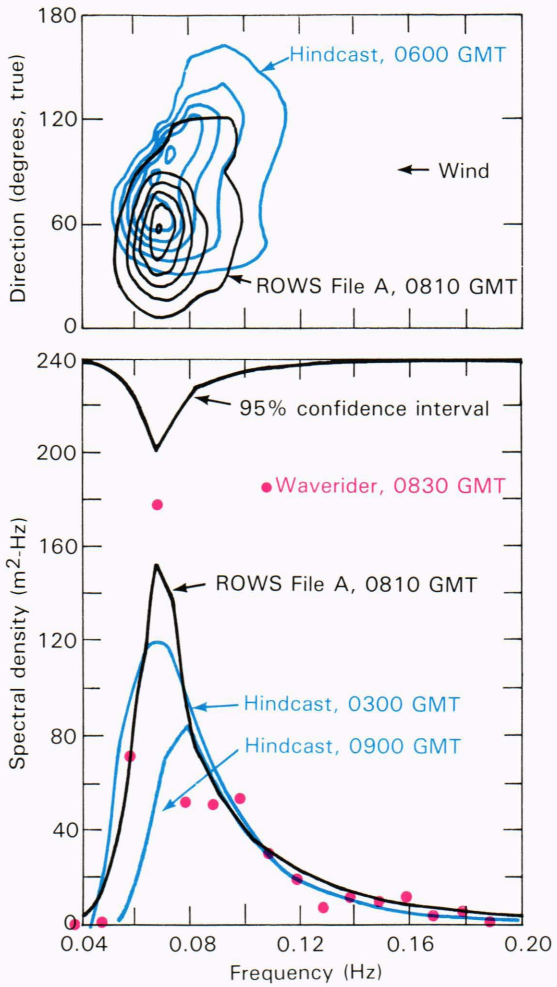

Figure 4—Comparison of ROWS, hindcast, and buoy spectra in the vicinity of ROWS file A (Fig. 2). The waverider spectrum is at 0830 GMT, the ROWS at 0810 GMT, and the hindcast times are as indicated. The curve at the top of the nondirectional comparisons is the ROWS 95 percent confidence interval. The significant wave height is 9.5 meters.

peak frequency is probably due to the slight fetch difference.

An excellent set of ROWS and SCR intercomparisons was obtained on the Chile SIR-B underflight mission in 1984. Some examples of these intercomparisons are given by Beal and by Monaldo (in this issue).

A ROWS MODE FOR SPECTRASAT

In Ref. 2, ROWS measurements are shown to be feasible at 700 kilometers altitude using a Seasat-class altimeter. However, the much lower altitude of Spectrasat offers some distinct advantages, first of which is the much smaller scan radius for the 275-kilometer Spectrasat altitude. For example, for a 12.5-degree nadir angle, the scan radius is about 60 kilometers. Thus, the greatest separation between the various directional cuts through the spectrum is 60 kilometers, this occurring between the fore/aft looks and the looks to broadside on either side of the satellite track. There are also some engineering advantages, including reduced transmitter-power requirements and increased contrast-signal levels for a given antenna gain.

There are a fair number of considerations and tradeoffs involved in designing a spaceborne system; at present, without a much more thoroughgoing "phase-A" type of study, we can offer only a preliminary conceptual system design. Among the more important design considerations are: incidence angle; twin-beam option for cross-section roll-off and wind vector determination; rotation rate and integration time; antenna and footprint dimensions; transmitter power, bandwidth, and pulse type and pulse-repetition frequency; and processor configuration, especially as driven by the requirements of geometrical correction and pulse integration for a fast-moving platform.

We will take as a given the basic transmitter and receiver characteristics described by MacArthur (in this issue) and repeated in Table 1. These will be seen to be adequate for the measurements.

Incidence Angle

There is a tradeoff between the best incidence angle for minimizing nonlinearities in the scattering and the small angle desired for minimizing the scan radius. At present, we only know theoretically that nonlinearities tend to be a minimum around 10 degree incidence; the best angle remains to be precisely determined for specified conditions of large wave steepness and wind speed (root-mean-square slope). Since this problem is not likely to be solved in the near future, we will simply settle for any earth-incidence angle in the neighborhood of 10 to 13 degrees. Since 13 degrees is the nominal incidence angle for the aircraft ROWS, we feel most comfortable with that angle. We note that at about 10 to 13 degrees incidence, the scattering cross section is nearly independent of wind speed (this is the well known "hinge point" in scatterometry). For the nominal 275-kilometer Spectrasat altitude, the scan radii corresponding to 10 and 13 degrees incidence are approximately 49 and 64 kilometers.

Twin Beam Option

The twin beam option is perhaps not so much an option as a requirement. While σ^0 at 10 to 13 degrees incidence is nearly independent of wind speed, the sensitivity coefficient varies by about a factor of 3 over the wind-speed range of 5 to 20 meters per second. If the scan radius were small enough, one could simply estimate the cross-section roll-off from the ratio of the radar altimeter's nadir σ^0 to the ROWS off-nadir σ^0, assuming a Gaussian slope probability density function, for example. (Note that in this case one can also simply use the radar altimeter wave-height estimate to scale the directional spectrum.) However, in the case of a 60 kilometer separation between the fore-and-aft and broadside looks, there can be a large wind variation, and hence a large mean-square slope and sensitivity variation. This problem can be solved (or substantially mitigated) by having an antenna with twin beams separated by one or two beamwidths in elevation, say, pointing to 10 and

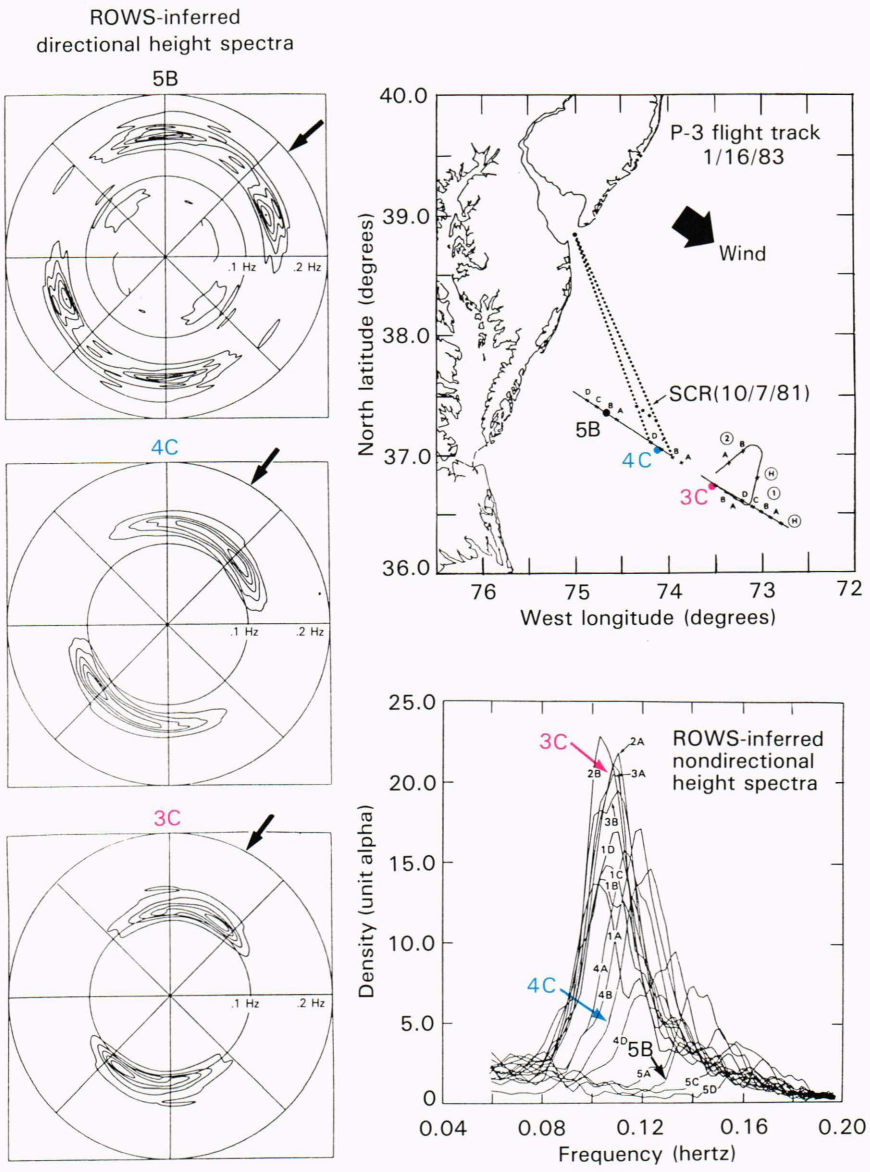

Figure 5—ROWS height-frequency spectra for fetch-limited waves off Wallops Island, Va., January 16, 1983. The contour levels are equally spaced in decrements of one-sixth the peak value. Neutral 10-meter winds were 13.9 meters per second. The top of the spectra corresponds to aircraft heading. The arrows in the representative directional spectra indicate directions from the center of the mouth of Delaware Bay.

13 degrees off nadir. While the looks will be only 15 kilometers apart, the cross-section roll-off will be appreciable. For example, according to Eqs. 3 and 4, for a 10-meter-per-second wind speed,

$$\frac{\partial \ln \sigma^0}{\partial \theta} \simeq \frac{-2 \tan \theta}{\langle (\nabla \zeta)^2 \rangle} = \frac{-2.3 \text{ dB}}{3^\circ} \text{ at } \theta = 11.5^\circ .$$

A twin-beam configuration will not only provide the cross-section roll-off for the sensitivity, but will at the same time provide wind-vector estimates, e.g., via the mean-square slope/wind-speed relationship of Eq. 3. (See Ref. 7 for a discussion of wind-vector measurements using scanning-beam scatterometers.)

Rotation Rate

The choice of rotation rate involves a tradeoff between the integration, or dwell time, and the density of coverage. We want the scan rate to be at least such that the spacecraft movement over a scan period T_{scan} is no more than the scan radius. For a 60-kilometer scan radius R, the rate required to produce measurement cells (i.e., areas containing 180 degrees of look on either of the satellite track) with commensurate along-track and cross-track dimensions is approximately 6 revolutions per minute (10-second period). Figure 7 shows the surface-scan patterns for three different rotation rates: 3, 6, and 12 revolutions per minute. It is seen that, for all rotation rates, if one allows less than 180 degrees of look for a measurement cell, the cell size can be reduced considerably. For example, in the 12-revolution-per-minute case, 120 degrees of the spectrum can be measured in about 35- to 40-kilometer cells to broadside on either side of the satellite track. Obviously, there are a number of ways the data from these scans could be treated. For the more rapid scans, i.e., for about 12 revolutions per minute or more, the coverage is dense enough to al-

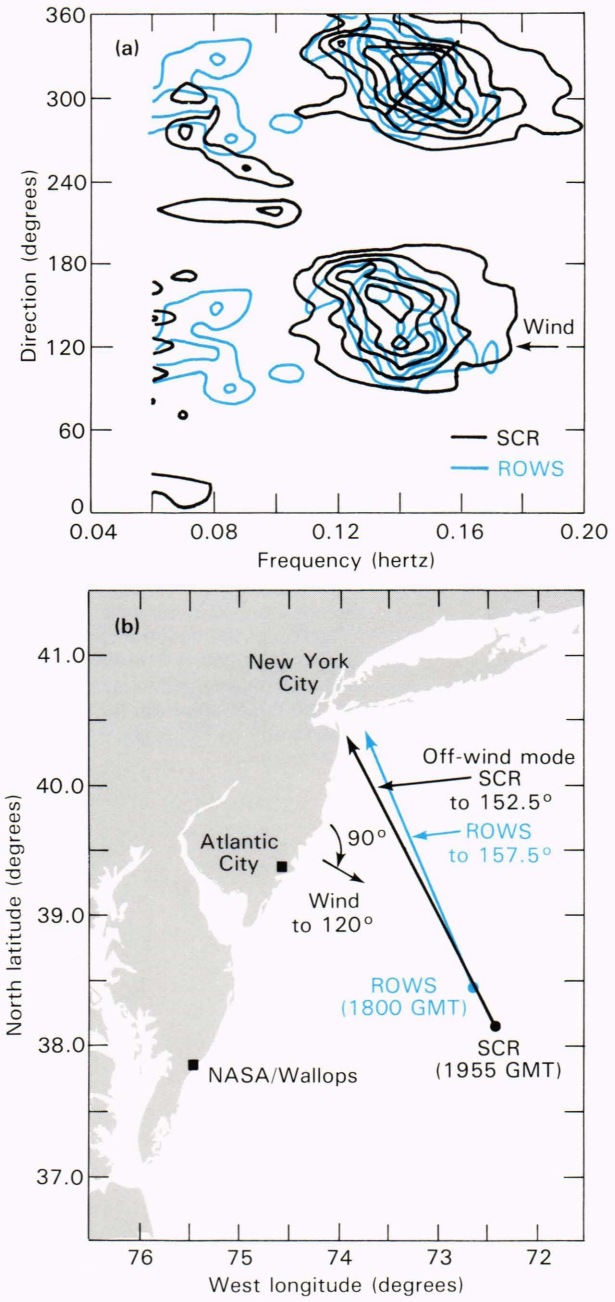

Figure 6—(a) Comparison of SCR and ROWS fetch-limited directional height-frequency spectra for a large fetch, January 18, 1983. The contours for both spectra are equally spaced in decrements of one-sixth the peak values. The off-wind component, directed to about 155 degrees T (true north), is traceable to the apex of the New York Bight as shown in (b), the accompanying map.

low a least-squares fitting of a locally linear field of $F(k,\phi)$ to the data, i.e., one could let the data

$$F(k_i,\phi_j;x_{jn},y_j) = F_{ijo} + \frac{\partial F_{ijo}}{\partial x}(x_{jn} - x_0) + \frac{\partial F_{ijo}}{\partial y} y_j ,$$

Table 1—Spectrasat ROWS characteristics.

Spacecraft altitude	275 km
Orbit	Near polar
ROWS antenna	Dual pencil beams, mechanically rotated, antenna type TBD
Total aperture	1 m × 1 m
Nadir angles	9.5° (beam 1) and 12.5° (beam 2)
RA/ROWS frequency	13.6 GHz
Beamwidth	1.6° azimuth × 1.6° elevation (each beam)
Antenna gain	37.8 dB effective/beam
Antenna scan rate	12 rpm
Surface scan radii	50 km and 65 km
RA/ROWS transmitter peak power	20 W
RA/ROWS transmit pulse	Linear FM, 320 MHz bandwidth chirped pulse, 16,384:1 pulse compression ratio
RA/ROWS pulse repetition frequency	4.1 kHz
ROWS mode peak power	18 W
ROWS receiving section IF filter bandwidth	60 MHz
Effective pulse length	9.6 μsec
Compressed pulse length	17 nsec
Detection	Square-law
SNR (thermal)	+6 dB
ROWS footprint (3 dB)	8 km × 8 km (each beam)
Surface range data window	6.4 km (each beam)
Surface range resolution	12 m
Geometrical correction	Optional
Surface range sampling	25 m × 256 at 6 bits (each beam)
Surface tracking	Input relative velocity vector
ROWS integration time	0.05 sec nominal
Modulation depth	16% rms nominal*
Signal-to-noise (output spectrum)	15 dB nominal; 0 dB minimum*
Directional resolution	5° nominal* (3-dB points)
Number of independent spectra per beam	~3 per 15° of azimuth
Output format	FNOC format 20% bandwidth wavenumber bins and 24 15° azimuth bins at 10 bits
Output bit rate	< 1 kilobit/sec
Degrees of freedom	~75 total for the 2 beams
Cell average degrees of freedom	~150 per 15° per 60-km cell

*Nominal = 200-m water wave, upwave/downwave looks, 10 m/sec wind speed; minimum = 50 m water wave at 3-dB points.

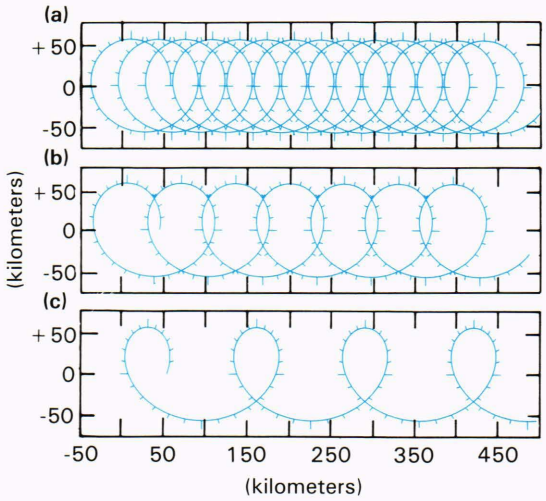

Figure 7—ROWS surface scan patterns (flat earth) for 250 kilometers altitude and 12.5 degrees nadir angle for scan rates of (a) 12 revolutions per minute, (b) 6 revolutions per minute, and (c) 3 revolutions per minute. The tic marks are for every 15 degrees of antenna rotation.

$$x_{jn} = VT_{\text{scan}}(\phi_j/2\pi + n) + R\cos\phi_j$$

$$y_j = R\sin\phi_j ,$$

where F is assumed to be symmetric, n is the scan number, $j = 1, 2, \ldots 24$ (say), and where the mean spectrum, F_0, and the gradient are to be evaluated at some center of mass, x_0, on the subsatellite track $y = 0$. We will see that a 12-revolution-per-minute scan does not limit the integration time; faster scans start to take a bite out of the output signal-to-noise ratio. Accordingly, for the present, we will take 12 revolutions per minute (72 degrees per second) as the nominal scan rate.

Antenna and Footprint Dimensions

The antenna gain requirement is set mainly by the minimum thermal signal-to-noise-ratio requirement and by the size of the range data window needed for a specified number of degrees of freedom in the spectral estimates. The azimuth footprint affects the signal strength only weakly as $L_y^{-1/2}$; further, the gain does not affect the output spectrum signal-to-noise ratio if the integration time is assumed to scale with the azimuth beamwidth, that is, if the integration time is limited by the requirement that the beam move no more than some fraction (e.g., one-half) of its azimuth footprint. Our original thinking was of an antenna having a 0.5-meter elevation by 1-meter-azimuth aperture, possibly of a Cassegrain design (see MacArthur, this issue). The antenna could also be a mechanically rotated planar array, either mechanically boresighted to off-nadir or electronically phased to off-nadir. This aperture would generate, at 13.6 gigahertz, a 3.2 degree elevation by 1.6 degree azimuth beamwidth. The broader elevation beamwidth was chosen mainly for the greater degrees of freedom afforded by the larger range data window (16 kilometers at 275 kilometers altitude). However, considering now the twin-beam configuration and the need for sufficient thermal signal-to-noise ratio for accurate cross-section roll-off measurements, the design problem becomes a little more complicated. For example, will the Cassegrain antenna work satisfactorily with dual subreflectors? Should the aperture now be significantly larger to increase the signal-to-noise ratio? Will some "noise-only" measurements suffice for the cross-section measurement, or should we have also a long-pulse mode for the cross-section measurements? Probably, noise-only measurements using, for example, a long sample gate before or after one of the main beam returns will suffice for the σ^0 measurements. The question of the antenna design will require some further thought. We will see from the discussion below that an approximately 1.6 degree pencil beam (1 meter × 1 meter aperture) is consistent with the simplest processor. If two such pencil beams are generated by beam switching, then the number of pulses, N, available for either beam must be halved; alternatively, if twin beams are generated simultaneously, the peak gain for each beam must be half that of a single beam generated by the 1 meter aperture since only half the transmitter power and half the collecting aperture area are effectively available for each beam, as can easily be seen by considering a phased array of discrete elements.

Integration Time, Sphericity Effects, and Processor Configuration

The number of independent pulses that can be averaged prior to the spectrum analysis of the detected range-reflectivity modulation signal depends on the Doppler bandwidth, B_d, of the backscattered signal, the pulse repetition frequency, and the antenna rotation rate or swell time, T_{int}, as discussed in Ref. 2. In addition, a limit on the integration time will be set by the wave-front curvature in azimuth and the platform velocity. The azimuth curvature is ultimately limiting because the curvature in the elevation plane can always be corrected for in the time-domain processing by using Eq. 8.[8]

If there is no geometrical correction, the surface wavenumber will vary over the range extent; i.e., the wavenumber will be dispersed according to Eq. 7. For $\beta_\theta = 1.6$ degrees, the wavenumber will be dispersed in the amount

$$\delta k/k = \cot\theta\,\beta_\theta = 0.12 ,$$

which is less than a standard wave-model band and therefore negligible. For larger elevation beamwidths, e.g., for $\beta_\theta = 3.2$ degrees, it will be necessary to correct the data geometrically according to Eq. 8. The wave-front sphericity (finite beamwidth) affects the integration time because of the differential range walk across the footprint (Fig. 8). If the beamwidth is small enough, the surface can be tracked accurately over the entire footprint simply by advancing or delaying the trigger on the waveform sampler according to

$$d\tau/dt = \dot{\tau}_0 = -(2V/c)\sin\theta_0\cos\phi_0 , \quad (10)$$

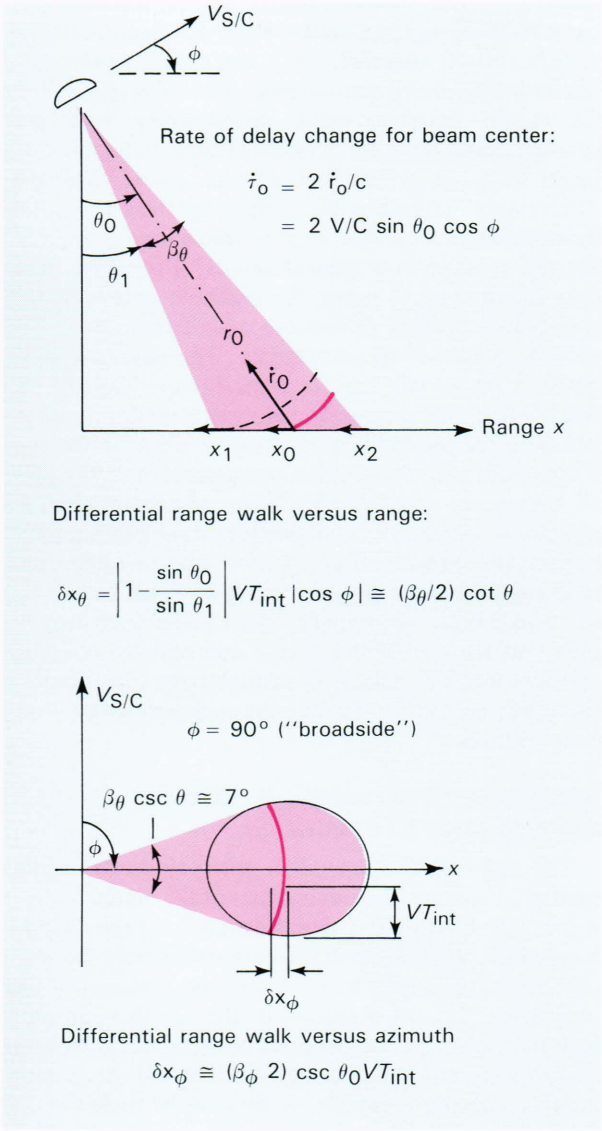

Figure 8—Differential range walk during the ROWS integration time T_{int} due to wave-front curvature, (top) in the elevation plane (range), and (bottom) in the horizontal plane (azimuth).

where V is the magnitude of the relative velocity vector between the radar and earth surface, and where the subscript refers to the center of the beam spot. For the given beamwidths, $\beta_\theta = \beta_\phi = 1.6$ degrees, the differential range walk over the integration time T_{int} is, from the elevation variation,

$$\pm\,\delta x_\theta = VT_{int}\,|\cos\phi_0|\,\cot\theta_0\,(\beta_\theta/2)$$

$$\lesssim 430 \text{ meters per second} \times T_{int}\ ,$$

and, from the azimuth variation,

$$\pm\,\delta x_\phi = VT_{int}\,|\sin\phi_0|\,\csc\theta_0\,(\beta_\phi/2)$$

$$\lesssim 430 \text{ meters per second} \times T_{int}\ ,$$

where V is assumed to be 7 kilometers per second. This range smearing must be kept less than the nominal surface range-sampling resolution, which we will take as 25 meters; say, less than 20 meters. Given these rates of slip, it is clear that the simplest ROWS system would have equal azimuth and elevation beamwidths of, say, 1.6 degrees and a fixed integration time of 0.05 seconds corresponding to the worst case $\delta x_\phi = 22$ meters at broadside ($\phi = 90$ degrees). It thus appears that the ROWS has its own kind of "azimuth fall-off" problem; however, it occurs in the SAR's *range* direction. In the case of the 1.6 degree beamwidth, there is no need for geometrical (sphericity) correction. For the case of 3.2 degree elevation beamwidth, geometrical correction is necessary for any integration time longer than about 0.02 second.

The limit on integration time of 0.05 second due to azimuthal wave-front curvature turns out to be no more severe than that due to beam rotation, since at a 12-revolution-per-minute scan rate, approximately one half of the subtended azimuth of 7 degrees is swept out during the integration time; i.e., 72 degrees per second $\times$ 0.05 second = 3.6 degrees. Interestingly, this corresponds almost exactly to the nominal 3-decibel spectral resolution for a 200-meter water wave according to Eq. 5, namely $\Delta\phi_{stat} = 3.6$ degrees; thus the spectral resolution for a 0.05-second integration time is conservatively approximately 5 degrees. We note that while the integration time might be varied according to azimuth, the increase in signal-to-noise ratio is not very significant (cf. the following and Table 1); further, by keeping T_{int} fixed, its effect on the sensitivity (through the dependence on the variable fraction of azimuth swept out during the integration time) is thereby eliminated.

If the Doppler bandwidth B_d is greater than the pulse repetition frequency (PRF), the number of independent pulses is given by $N = PRF \times T_{int}$: if the bandwidth is less, $N = B_d \times T_{int}$. Since for the pulse limited geometry,

$$B_d = (2V/\lambda_{em})\,|\sin\phi|\,\beta_\phi = 18 \text{ kilohertz}\,|\sin\phi|$$

exceeds the pulse repetition frequency (= 4 kilohertz) for all azimuths outside of 12 degrees of fore and aft, we have for most azimuths

$$N = 4 \text{ kilohertz} \times 0.05 \text{ second} = 200\ .$$

Figure 9 is a block diagram of a ROWS system with a processor based on straightforward pulse integration. Figure 10 depicts the RA/ROWS pulse returns and waveform sampler trigger sweeps. As discussed by MacArthur (this issue), the 320 megahertz bandwidth RA/ROWS signal cannot be compressed in the ROWS receiving section using the full de-ramp technique, since far too many range bins are required. Thus, the received ROWS mode signal is filtered to 60 megahertz bandwidth and dechirped using a surface acoustic wave device. The surface range resolution then becomes $\Delta x =$

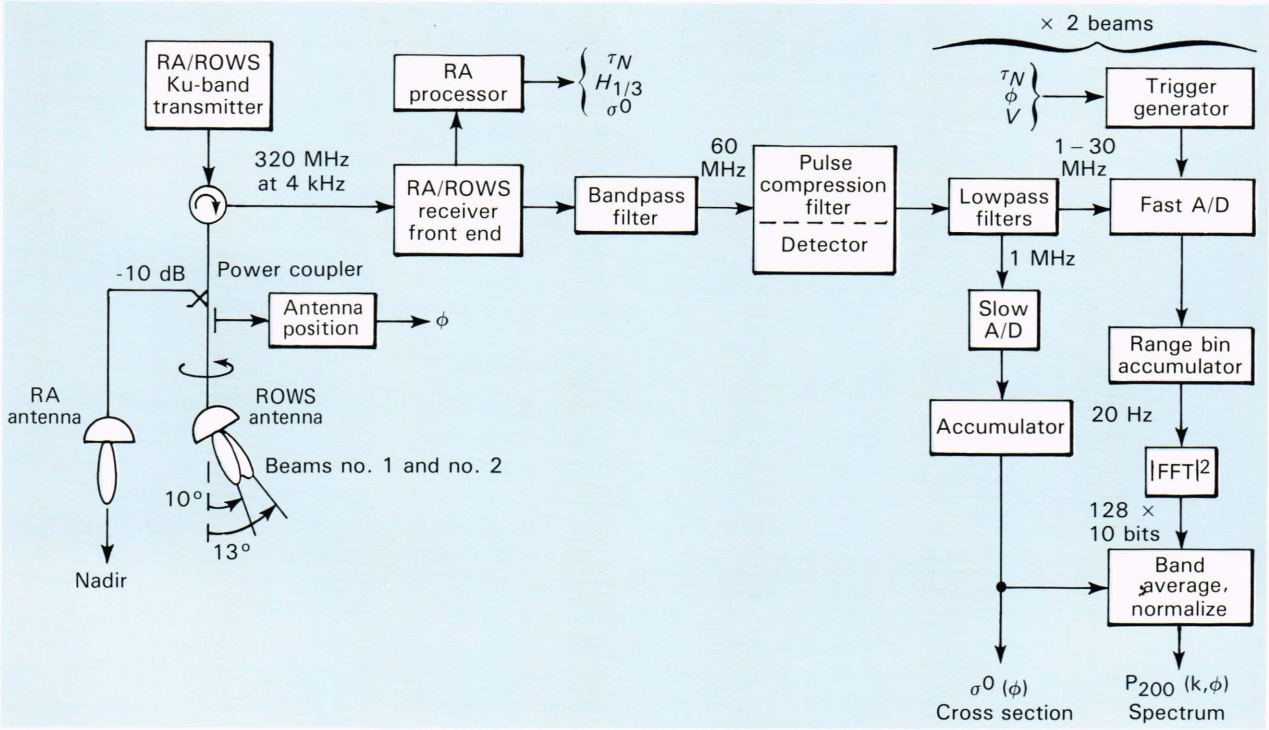

Figure 9—Block diagram of Spectrasat radar altimeter/spectrometer (RA/ROWS) subsystems with the ROWS-mode time-domain processor (tracker and integrator).

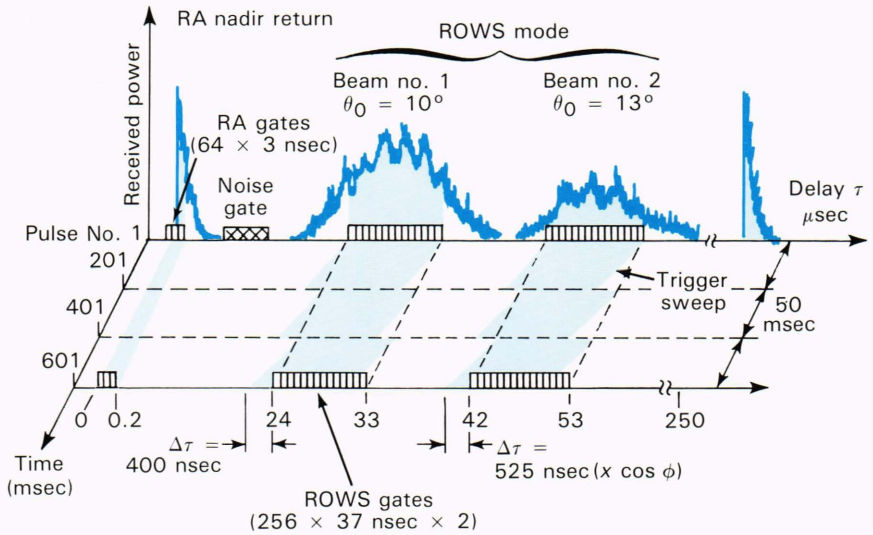

Figure 10—RA/ROWS pulse return versus delay time (range) and pulse number, and ROWS trigger sweeps. (The location of the noise gate is illustrative only.)

12 meters. After detection, the signal is further conditioned with a 30-megahertz filter to permit sampling at 25 meters resolution (37-nanosecond gates). Since 75 percent of the signal energy is lost and the excess bandwidth that could have been used for speckle reduction is not utilized, this design is clearly not ideal; however, it does give the general flavor of a RA/ROWS system design. For the twin-beam design, two 256 six-bit samplers, each triggered with a variable delay according to Eq. 10, will provide at 37 nanoseconds resolution a total of 2 × 256 × 25 meters = 12.8 kilometers of range record for the modulation signal. Since the 3-decibel spectral window width in azimuth for 0.05 second integration is about 5 degrees, there will be approximately three independent spectral estimates for every 15 degrees of azimuth; assuming logarithmically spaced 20 percent (approximately) wavenumber bands, we should then have about 75 degrees of freedom per 15-degree azimuth bin for a nominal 200-meter water wave.

While the conceptual design here is based on a straightforward pulse integration, the possibility of alternative processing schemes should not be discounted. For example, if the radar-to-earth-surface relative velocity vector were not precisely known, a processor could be used that spectrum-analyzed the Doppler-shifted modulation signal over a number of slow-frequency

bands, $\Omega_i = \mathbf{k}_i \cdot \mathbf{V}_{rel}$, that would cover with certainty the Doppler shift frequencies of the modulation signal. This processing would be similar to that proposed in Ref. 4 for the two-frequency technique.

PERFORMANCE SUMMARY

The proposed ROWS system and performance characteristics have been given above in Table 1. Table 2 details the link equation for the thermal signal-to-noise ratio. The measurement signal-to-noise ratio is calculated assuming a Phillips spectrum,

$$F(\mathbf{k}) = Bk^{-4}\,(4/3\pi)\cos^4\phi\ ,$$

with $B = 0.005$ and assuming a nominal wind speed of 10 meters per second for the α estimate. Both the thermal signal-to-noise ratio and the output spectrum signal-to-noise ratio are seen to be quite good. For example, for the shortest sampled wavelength, 50 meters, the signal-to-noise ratio is unity at the directional half-power points. In Table 1, the "cell-average" degrees of freedom is based on the approximate two scans in the nominal 60 by 60 kilometer cell. This gives approximately four spectral samples for fore and aft looks if there is no overlap and two samples for broadside looks. However, we will probably want to design for 100 percent overlap of fore and aft looks in order to develop a database for modeling 180-degree asymmetries in the modulation spectra caused, for example, by skewness in the wave-slope distribution.

Apart from the sampling errors, the magnitude of which may be inferred from the degree-of-freedom estimates in Table 1, no error or accuracy figures are given for the system. On the basis of the aircraft data analyzed so far, however, in the energy-containing part of the spectrum, an accuracy on the order of the sampling error might be expected; quoting more precise numbers would at this point not be very meaningful. (For example, the 16-centimeter root-mean-square error in significant wave height found in Ref. 2 for a 2 to 10 meter range is based on only seven cases.)

CONCLUSION

The ROWS technique has been described, some examples have been given of the aircraft data, and a straw-man conceptual design for a ROWS mode on Spectrasat has been presented. The expected performance of the system is seen to be quite good. The low altitude of Spectrasat offers some engineering advantages, particularly in terms of reduced transmitter power and antenna gain; more important, however, is the much tighter scan pattern for the low-altitude orbit. One is here getting down to the scale of the aircraft observations of Fig. 2, and one should be able to apply the ROWS data usefully to a variety of geophysical situations.

We have indicated the need for two elevation beams in order to measure the cross-section roll-off both for the sensitivity calculation and for wind vector estimates. Although we have not had a chance to consider what type of antenna such an option might imply, one does

Table 2—ROWS SNR (thermal).*

Parameter	*Value*	*Factor*	*Decibels*
Peak power W_t*	18 W		42.6 (mW)
Antenna gain G*	37.8	G^2	75.6
Wavelength, λ	0.022 m	λ^2	− 33.2 (m^2)
Pulse length, τ	9.6 μsec		
Incidence angle, θ_E	13.1°	$(c\tau/2 \sin\theta_E)$	38.0 (m)
Azimuth beamwidth, β_θ	1.6°	0.028 rad	− 15.5
Cross section, σ^0	+ 5 dB		+ 5
			+112.5
Slant range, R	282 km	$(4\pi R)^3$	196.4 (m^3)
Noise power, kT	4×10^{-21} W/Hz		
Bandwidth B	60 MHz		
Noise factor, F	4 dB	kTBF	− 92.3 (mW)
Loss factor, L			2
		(−)	+106.1
		SNR =	+ 6.4 dB

*For the twin-beam configuration, the power can be considered 9 W for each beam where the collecting aperture per beam is 0.5 m × 1 m; equivalently, the effective one-way gain can be considered halved for each beam in the link equation as is done here.

$$\text{SNR} = \frac{W_t G^2 \lambda^2 (c\tau/2 \sin\theta_E)\beta_\phi \sigma^0}{(4\pi R)^3 (kTBF)L}$$

not imagine that this would present any real engineering difficulties.

We have seen that a limit on the ROWS integration time of about 0.05 second is imposed by wave-front curvature and beam rotation effects; for integration times approaching that limit, there will be a loss of high-frequency response that must be accounted for along with the point-target pulse response by the appropriate inverse filter.

Many considerations, tradeoffs, and options are obviously involved in the design of a ROWS system for space, and, clearly, a "phase-A" type of study effort will be required before a more definitive design can be offered.

Presently, on the basis of aircraft data analyzed so far, we are fairly confident about the accuracy of the measurements for sea states greater than 2 meters and wind speeds greater than 5 meters per second. Continued analysis and intercomparison of aircraft ROWS spectra with buoy and SCR spectra will help to better quantify the limits of accuracy of the ROWS spectra produced according to the linear tilt model. However, it is important to note that, whatever the errors in the inferred spectra, they are generally relatively small, and a reasonable scattering theory exists upon which one may base more sophisticated algorithms to mitigate these errors (cf. accompanying paper by the same author, this issue).

REFERENCES and NOTE

[1] F. C. Jackson, "An Analysis of Short Pulse and Dual Frequency Radar Techniques for Measuring Ocean Wave Spectra from Satellites," *Radio Sci.* **16**, 1385-1400 (1981).

[2] F. C. Jackson, W. T. Walton, and P. L. Baker, "Aircraft and Satellite Measurement of Ocean Wave Directional Spectra Using Scanning-Beam Microwave Radars," *J. Geophys. Res.* **90**, 987-10004 (1985).

[3] F. C. Jackson, W. T. Walton, and C. Y. Peng, "A Comparison of in situ and Airborne Radar Observations of Ocean Wave Directionality," *J. Geophys. Res.* **90**, 1005-1018 (1985).

[4] W. Alpers and K. Hasselmann, "The Two-Frequency Microwave Technique for Measuring Ocean Wave Spectra from an Airplane or Satellite," *Boundary-Layer Meteorol.* **13**, 215-230 (1978).

[5] F. C. Jackson, "On the Wind Speed Dependence of Sea-Surface Mean Square Slope," Sixth Conference on Air-Sea Interaction (Jan 13-17, 1986).

[6] E. J. Walsh, D. W. Hancock III, D. E. Hines, and J. E. Kenney, "Development of the Fetch-Limited Directional Wave Spectrum," *Oceans '82 Conference Record*, pp. 820-825 (1982).

[7] T. Kiramoto and R. K. Moore, "Scanning Wind Vector Scatterometers with Two Pencil Beams," in *Frontiers of Remote Sensing of the Oceans and Atmosphere from Air and Space Platforms*, NASA Conference Publication 2303, pp. 89-104 (Feb 1984).

[8] This limitation was recently pointed out to me by J. MacArthur and I confess I was taken aback for not seeing it before (e.g., in Refs. 2 and 3); however, in going back to Ref. 1, I see that the effect is actually modeled by Eqs. 8, 52, 56, and 57.